CrystEngComm

RSC Publishing

PAPER

The first molecular superconductor based on BEDT-TTF radical cation salt with paramagnetic tris(oxalato)ruthenate anion†

Cite this: *CrystEngComm*, 2013, **15**, 7048

Tatiana G. Prokhorova,*[a] Leokadiya V. Zorina,[bc] Sergey V. Simonov,[bc] Vladimir N. Zverev,[bc] Enric Canadell,[d] Rimma P. Shibaeva[b] and Eduard B. Yagubskii*[a]

Received 24th May 2013,
Accepted 11th July 2013

DOI: 10.1039/c3ce40919h

www.rsc.org/crystengcomm

The first molecular superconductor based on BEDT-TTF radical cation salt with the paramagnetic tris(oxalato)ruthenate anion, β′′-(BEDT-TTF)$_4$K$_x$(H$_3$O)$_{1-x}$[Ru^{III}(ox)$_3$]C$_6$H$_5$Br ($x \sim 0.8$), is synthesized and its crystal and electronic structure as well as transport and magnetotransport properties are studied. The single crystals have monoclinic *C*2/*c* symmetry and β′′-packing of the conducting BEDT-TTF layer. The samples were found to be superconductors with T_c = 2.8–6.3 K (depending on the sample). Well pronounced Shubnikov–de Haas oscillations are observed in the field range 7–17 T. The Fourier spectrum of the oscillations mainly consists of two frequencies, which correspond to the Fermi surface cross sections 6.3% and 0.85% of the Brillouin zone. The first one with good accuracy corresponds to the calculated cross section 7.5%, the origin of the second one is discussed. Semiconducting orthorhombic phase 'pseudo-κ'-(BEDT-TTF)$_4$K$_x$(H$_3$O)$_{1-x}$[Ru^{III}(ox)$_3$]C$_6$H$_5$CN is also synthesized and studied.

Introduction

The largest known family of hybrid bifunctional molecular crystals based on BEDT-TTF (bis(ethylenedithio)tetrathiafulvalene) radical cation salts with paramagnetic tris(oxalato)metalate anions (BEDT-TTF)$_4$A^I[M^{III}(ox)$_3$]G, where M^{III} is Fe, Cr, Mn; A^I is H$_3$O$^+$, NH$_4^+$, K$^+$, Rb$^+$; G is the guest solvent molecule, has been investigated over the past 20 years.[1–17] During this time four polymorphous modifications of salts of this family were discovered. These polymorphs differ in symmetry (monoclinic, orthorhombic, triclinic), and/or the packing type of conducting layers, as well as the distribution of the enantiomers of a chiral anion [M(ox)$_3$]$^{3-}$ in alternating anionic layers. These structural differences lead to different physical properties. The formation of crystals of one or other polymorphous modification depends on the nature, size and shape of the guest solvent molecules and the conditions of electrochemical synthesis.

The orthorhombic group of the crystals involves five semiconductors with 'pseudo-κ' packing of conducting layers (M = Fe^{III}, Cr^{III}; A = K$^+$, NH$_4^+$, H$_3$O$^+$; G = PhCN and its mixtures with PhNO$_2$ or 1,2-C$_6$H$_4$Cl$_2$).[1,6,13]

The triclinic group includes two bi-layered polymorphs, in which conducting layers with α-β′′- or α-'pseudo-κ'-types of packing alternate.[10,11,13,14] These crystals may be of interest to study the mechanism of the interlayer transport and effects of the interaction between the conducting layers with different types of radical cation packing.

However, now the group of monoclinic crystals with β′′-type packing of BEDT-TTF radical cations[1–9,12,17] are of the most interest among the family of salts. The conducting properties of monoclinic phases vary from semiconducting to metallic and superconducting by changing the guest solvent molecule G. The superconducting phases were formed when G is PhCN, PhNO$_2$, PhBr, PhF and DMF (dimethylformamide) as well as mixtures of PhCN with PhCl, PhBr, 1,2-C$_6$H$_4$Cl$_2$ and C$_5$H$_5$N.[1,2,4,8,12,13,16,17] Other samples of β′′-salts with G = PhCl, C$_5$H$_5$N and 1,2-C$_6$H$_4$Cl$_2$ show metallic behaviour without a superconducting transition down to 1.5 K.[3,8,9,13] The temperature dependencies of the resistivity of β′′-salts with G = CH$_2$Cl$_2$ and PhI are semiconducting.[5,17] A more detailed study of the structure and conducting properties of monoclinic crystals revealed that a structural phase transition from monoclinic *C*2/*c* to triclinic *P*$\bar{1}$ symmetry takes place at 180–230 K in a number of crystals where G is halobenzene (PhF, PhCl, PhBr, 1,2-C$_6$H$_4$Cl$_2$) and their mixtures with benzonitrile.[15,17] The investigation of magnetic properties of monoclinic β′′-(BEDT-TTF)$_4$NH$_4$[Cr(ox)$_3$]·DMF crystals shows that there is an interaction between π-electrons of the conducting sublattice and d-electrons of the magnetic one.[18]

[a]*Institute of Problems of Chemical Physics, RAS, Chernogolovka, MD, 142432, Russia. E-mail: prokh@icp.ac.ru; yagubski@icp.ac.ru*
[b]*Institute of Solid State Physics, RAS, Chernogolovka, MD, 142432, Russia*
[c]*Moscow Institute of Physics and Technology, Dolgoprudny, Moscow Region, Russia*
[d]*Institut de Ciència de Materials de Barcelona, CSIC, Campus de la UAB, E-08193 Bellaterra, Spain*

† Electronic supplementary information (ESI) available. CCDC 937885 and 937886. For ESI and crystallographic data in CIF or other electronic format see DOI: 10.1039/c3ce40919h

It is particularly remarkable that all the salts of this family described so far contain paramagnetic complex anions of 3d-elements only. It is of interest to synthesize the salts of BEDT-TTF with tris(oxalato)metalate anions of 4d- and 5d-metals, the magnetic properties of which are different from those of 3d-elements due to the presence of spin–orbit interaction.

In this work we report on the synthesis, crystal and electronic structure as well as transport and magnetotransport properties of the first BEDT-TTF salts with tris(oxalato)ruthenate anion: the superconducting monoclinic phase β′′-(BEDT-TTF)$_4$K$_x$(H$_3$O)$_{1-x}$[Ru^{III}(ox)$_3$]C$_6$H$_5$Br (**1**) with T_c = 2.8–6.3 K (depending on the sample) and the semiconducting orthorhombic phase 'pseudo-κ'-(BEDT-TTF)$_4$K$_x$(H$_3$O)$_{1-x}$[Ru^{III}(ox)$_3$]C$_6$H$_5$CN (**2**), where $x \sim 0.8$ in **1** and 0.7 in **2**.

Experimental

Synthesis of starting materials and radical cation salts

BEDT-TTF, C$_6$H$_5$Br, C$_6$H$_5$CN, and 1,2,4-C$_6$H$_3$Cl$_3$ were used as received (Aldrich); 18-crown-6 (Aldrich) was purified by recrystallization from acetonitrile and dried in vacuum at 30 °C over P$_2$O$_5$; K$_3$[Ru(ox)$_3$]·4.5H$_2$O was synthesized according to a procedure described in ref. 19.

Electrocrystallization of the charge transfer salts was performed in conventional two-compartment H-shaped cells with Pt wire electrodes at a constant current of 0.75 μA and at a constant temperature of 25 °C. The dissolution of the electrolyte K$_3$[Ru(ox)$_3$]·4.5H$_2$O and BEDT-TTF at ∼60 °C was performed in a different compartment of the cell, as oxidation of BEDT-TTF by a metal complex anion takes place at elevated temperature. The exact conditions for the synthesis of each salt are described below.

Synthesis of crystals (1). 100 mg of K$_3$[Ru(ox)$_3$]·4.5 H$_2$O and 200 mg of 18-crown-6 were placed in the cathode compartment; 16 mg of BEDT-TTF was placed in the anode one. The mixture of bromobenzene (20 ml) with 96% ethanol (2 ml) was used as a solvent and distributed between the two compartments of the cell. Several crystals in the form of parallelepipeds were collected from the anode after 3 weeks.

Synthesis of crystals (2). 190 mg of K$_3$[Ru(ox)$_3$]·4.5 H$_2$O together with 380 mg of 18-crown-6 were placed in the cathode compartment; 15 mg of BEDT-TTF was placed in the anode one. The mixture of 1,2,4-trichlorbenzene (10 ml), benzonitrile (10 ml) and 96% ethanol (2 ml) was distributed between the two compartments of the cell. The many crystals of small size in the form of parallelepipeds were collected from the anode after 3 weeks.

Crystal structure determination

X-ray single crystal diffraction data were collected on an Oxford Diffraction Gemini-R diffractometer at room temperature using Mo Kα radiation [λ(Mo Kα) = 0.71073 Å, graphite monochromator, ω-scans]. Data reduction with empirical absorption correction of experimental intensities (Scale3AbsPack program) was made with the CrysAlisPro software.[20]

The structures were solved by a direct method followed by Fourier syntheses and refined by a full-matrix least-squares method in an anisotropic approximation for all non-hydrogen atoms using the SHELX-97 programs.[21] Hydrogen atoms in BEDT-TTF and solvent molecules were placed in idealized positions and refined using a riding model, U_{iso}(H) were fixed at 1.2U_{eq}(C). K$^+$ cation and oxygen atom of the H$_3$O$^+$ cation were placed in the same position within the anion layer and their relative occupancies were refined as combination of x and $(1 - x)$. H atoms in the hydroxonium H$_3$O$^+$ cations were not located but included into the chemical formula of the compounds **1** and **2**.

Crystal data for 1. C$_{52}$H$_{37.57}$BrK$_{0.81}$O$_{12.19}$RuS$_{32}$, M = 2096.00, T = 293(2) K, monoclinic, a = 10.2882(5), b = 19.973(1), c = 35.485(2) Å, β = 93.483(5)°, V = 7278.2(7) Å^3, $C2/c$, Z = 4, D_{calc} = 1.913 g cm^{-3}, μ = 17.88 cm^{-1}, $2\theta_{max}$ = 64.64°, 38 027 reflections measured, 12 106 unique reflections (R_{int} = 0.0272), 10 051 reflections with $I > 2\sigma(I)$, 518 parameters refined, R_1 = 0.0431, wR_2 = 0.0914, GOF = 1.020.

Crystal data for 2. C$_{53}$H$_{37.93}$K$_{0.69}$NO$_{12.31}$RuS$_{32}$, M = 2039.70, T = 293(2) K, orthorhombic, a = 10.3683(4), b = 19.6056(9), c = 36.083(1) Å, V = 7334.9(5) Å^3, $Pbcn$, Z = 4, D_{calc} = 1.847 g cm^{-3}, μ = 12.24 cm^{-1}, $2\theta_{max}$ = 61.14°, 85 062 reflections measured, 10 602 unique reflections (R_{int} = 0.0455), 7891 reflections with $I > 2\sigma(I)$, 473 parameters refined, R_1 = 0.0522, wR_2 = 0.1103, GOF = 1.018.

Electronic band structure calculations

The tight-binding band structure calculations[22] were of the extended Hückel type. A modified Wolfsberg–Helmholtz formula was used to calculate the non-diagonal $H_{\mu\nu}$ values.[23] All valence electrons were taken into account in the calculations and the basis set consisted of Slater-type orbitals of double-ζ quality for C 2s and 2p, S 3s and 3p and of single-ζ quality for H1s. The ionization potentials, contraction coefficients and exponents were taken from previous work.[24]

Conductivity and magnetotransport measurements

The transport measurements in the temperature range (0.4–300 K) were carried out in a cryostat with a superconducting solenoid, which generated a magnetic field of up to 17 T. The temperature dependencies of the electrical resistance of single crystals were measured using a four-probe technique by a lock-in detector at 20 Hz alternating current in the range (1–10) μA. Two contacts were attached to each of two opposite sample surfaces with conducting graphite paste. In the experiment we have measured the out-of-plane resistance $R_\perp$ with the current running perpendicular to the conducting layers. Because of the high anisotropy of the samples we did not succeeded in the measurements of the in-plane sample resistance.

Results and discussion

Synthesis

It should be noted, that up to now only one radical cation salt with [Ru^{III}(ox)$_3$]$^{3-}$ anion was reported, namely, the (TTF)$_3$[Ru^{III}(ox)$_3$](C$_2$H$_5$OH)$_{0.5}$·4H$_2$O containing isolated

anions.[25] The known attempts to synthesize the crystals based on BEDT-TTF with $[Ru^{III}(ox)_3]^{3-}$ in the medium of the wet solvent (benzonitrile) and in the presence of the $K_3[Ru(ox)_3]4.5H_2O$ or $(NH_4)_3[Ru(ox)_3]1.5H_2O$ as electrolytes described in the literature[6] were unsuccessful. Previously,[13] we have shown that the addition of 96% ethanol and 1,2,4-triclorobenzene to the reaction medium promotes the formation of high quality monoclinic crystals of the family, increasing the crystal growth rate, the reproducibility and selectivity of the electrocrystallization process. In the present work we used two different mixtures of solvents: bromobenzene with 96% ethanol and benzonitrile with 96% ethanol and 1,2,4-triclorobenzene. The $K_3[Ru(ox)_3]4.5H_2O$ salt was employed as electrolyte. The crystals of the superconducting monoclinic phase were obtained with G = bromobenzene (**1**), while in the case of G = benzonitrile the orthorhombic semiconducting crystals (**2**) formed.

Crystal structures

β′′-(BEDT-TTF)$_4$K$_x$(H$_3$O)$_{1-x}$[Ru(ox)$_3$]PhBr, x = 0.81 (1, sample with maximal T_c). Compound **1** belongs to the monoclinic series of the (BEDT-TTF)$_4$A[M(ox)$_3$]G family. The monoclinic lattice of *C*2/*c* symmetry contains two independent BEDT-TTF donors (A and B) in general positions, one mixed $[K_x(H_3O)_{1-x}]^+$ cation and one $[Ru(ox)_3]^{3-}$ anion in special positions on a two-fold axis and one solvent bromobenzene molecule disordered in two equiprobable sites near the two-fold axis. One of the two BEDT-TTF donors (A) is fully ordered in an eclipsed conformation while both terminal ethylene groups of another donor (B) are disordered between two positions with 0.69/0.31 and 0.67/0.33 occupancies.

Projection of the crystal structure **1** along the *a*-direction is shown in Fig. 1. The structure consists of the conducting layers of BEDT-TTF radical cations alternating with mixed anion–solvent layers along the crystallographic *c*-axis. The conducting radical cation layer has a well-known β′′-type of the molecular packing and is composed of parallel BEDT-TTF stacks. Central C=C bonds of two independent BEDT-TTF show no difference in bond lengths which are both equal to 1.364(3) Å. This indicates identical charge state of the two radical cations, BEDT-TTF$^{0.5+}$ according to the chemical formula. There are shortened S···S intermolecular contacts along and between the stacks which are discussed below in the Electronic structure section.

Complex anion layers of the $\{[K_x(H_3O)_{1-x}]^+[Ru(ox)_3]^{3-}PhBr\}^{2-}$ composition include paramagnetic Ru^{III} oxalate anions, small singly-charged cations and neutral solvent molecules. K^+ and H_3O^+ cations are mixed in the same site and their relative occupation factors were refined to 0.81 and 0.19, respectively. The structure of the anion layer has a honeycomb-like geometry (see Fig. S2 in ESI†), one hexagonal motif of the layer is shown in Fig. 2a. Ru^{3+} and K^+/H_3O^+ cations are alternated in vertexes of a slightly distorted hexagonal network and linked by oxalate bridges along the sides of hexagons. Guest solvent molecules fill hexagonal cavities of the layer. Every anion layer is represented by combination of only right or only left isomers of the chiral $[Ru(ox)_3]^{3-}$ anion, the layers of different chirality are repeated alternately along the *c*-direction. Both Ru and K^+/H_3O^+ centers are coordinated by six oxygen atoms. One of three independent Ru–O bond distances in the anion of 2.031(2) Å is shorter than two others of 2.048(2) Å. The same observation concerns distances between K^+/H_3O^+ and oxygen which are equal to 2.762(2), 2.926(3) and 2.960(3) Å. Aromatic ring of the solvent molecule is shifted inside the cavity to A^+ cation opposite to the Br substituent and lies between two parallel oxalate ligands of the $[Ru(ox)_3]^{3-}$ anion elongated along *b*. The dihedral angle between mean planes of these oxalate groups and bromobenzene is 86.6(1)°.

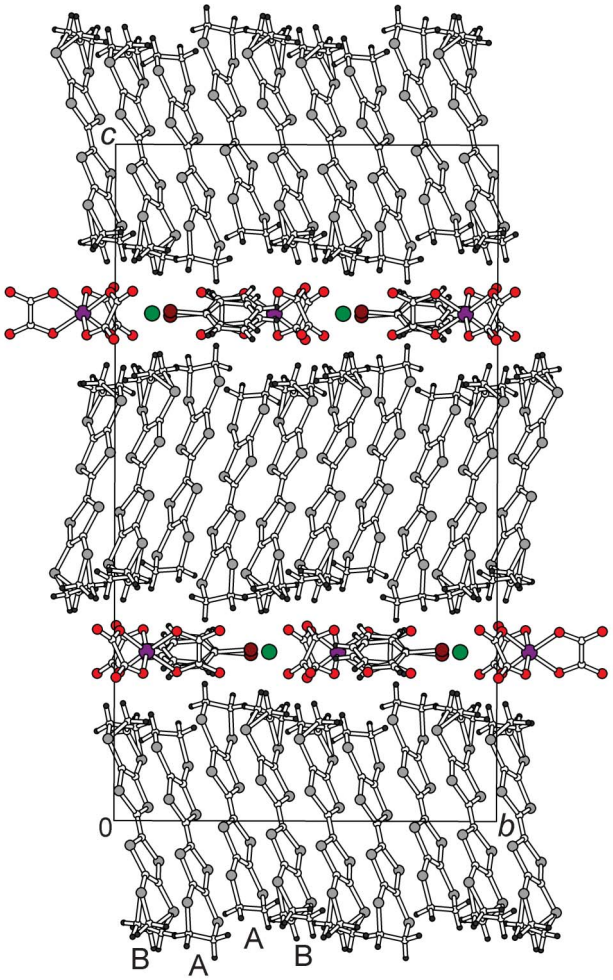

Fig. 1 Crystal structure of β′′-(BEDT-TTF)$_4$K$_x$(H$_3$O)$_{1-x}$[Ru(ox)$_3$]PhBr (**1**) projected along the *a*-axis. A and B letters refer to two independent BEDT-TTF donors.

Donor···anion hydrogen contacts are somewhat shorter for the disordered ethylene group sites with major occupation (H_{et}···O_{ox} distances are 2.42, 2.44 and 2.46 Å) than for the sites with minor occupation (2.45, 2.50, 2.47, 2.53 Å). Ordered donor forms one H···O contact with oxygen of the oxalate group of 2.50 Å. H···O contacts between solvent and the anion are 2.54, 2.58 and 2.59 Å; Br atom of the solvent lies on the distance of 3.02–3.03 Å from nearest H atoms of the donor. Geometry and values of the hydrogen contacts are close to those found in another superconducting salt of the family (T_c = 4.0 K) with G = PhBr, where M = Fe^{3+}, A = H_3O^+.[26] Unit cell

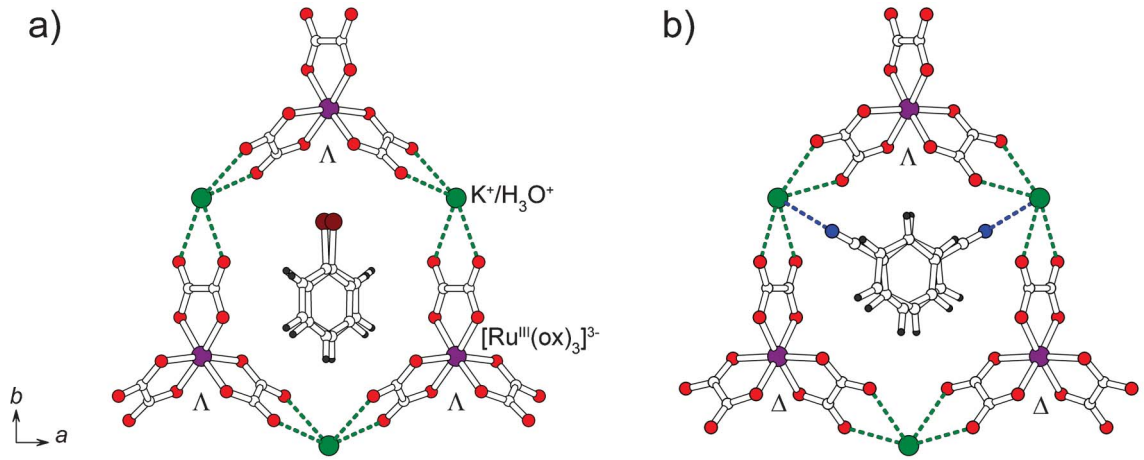

Fig. 2 Hexagonal motif of the honeycomb-like anion layer in monoclinic *C*2/*c* structure **1** (a) and orthorhombic *Pbcn* structure **2** (b).

parameters of the salt **1** are practically identical to those for the other superconductor of the family with PhBr, H_3O^+ and Cr^{3+} (T_c = 1.5 K);[8] the unit cell volume difference is only 1 Å^3.

'Pseudo-κ'-(BEDT-TTF)$_4$K$_x$(H$_3$O)$_{1-x}$[Ru(ox)$_3$]PhCN, x = 0.69 (2). The radical cation salt **2** belongs to the orthorhombic series (space group *Pbcn*) and differs from the monoclinic salt **1** by internal structure of both radical cation and anion layers.

The asymmetric unit of the structure **2** contains two independent fully ordered BEDT-TTF molecules, half mixed K^+/H_3O^+ cation and half the ruthenium oxalate anion in the position on a two-fold axis, and half benzonitrile molecule disordered around a two-fold axis. Terminal ethylene groups of two donors are ordered and have eclipsed conformation.

The conducting BEDT-TTF layer shown in Fig. 3 has the 'pseudo-κ' type of the molecular packing which was observed before in other members of the orthorhombic series of the (BEDT-TTF)$_4$A^{I}[M^{III}(ox)$_3$]G family with M = Fe and G = PhCN,[1,6] (PhCN)$_{0.88}$(C$_6$H$_4$Cl$_2$)$_{0.12}$,[13] (PhCN)$_{0.8}$(PhNO$_2$)$_{0.2}$;[13] M = Cr, Co, Al and G = PhCN.[6] It consists of face-to-face BEDT-TTF dimers each of which is surrounded by six monomeric units. Charge state of the BEDT-TTF radical cation composing the dimer is close to 1+ according to valence bond distances distribution; central C=C bond length in TTF is elongated to 1.386(4) Å. BEDT-TTF in the monomer is neutral and the corresponding C=C bond length is as short as 1.340(4) Å. Besides, the molecule of the monomer is more strongly bent in comparison with the radical cation of the dimer, corresponding dihedral angles of bending across S–S lines are 9.65(5) and 8.47(6)° in the monomer against 1.92(5) and 2.54(5)° in the dimer that also indicates difference in charge. Due to the charge localization inside the dimers, the salt **2** shows semiconducting behavior as all other salts of the (BEDT-TTF)$_4$A^{I}[M^{III}(ox)$_3$]G family with 'pseudo-κ' packing of the conducting layer.

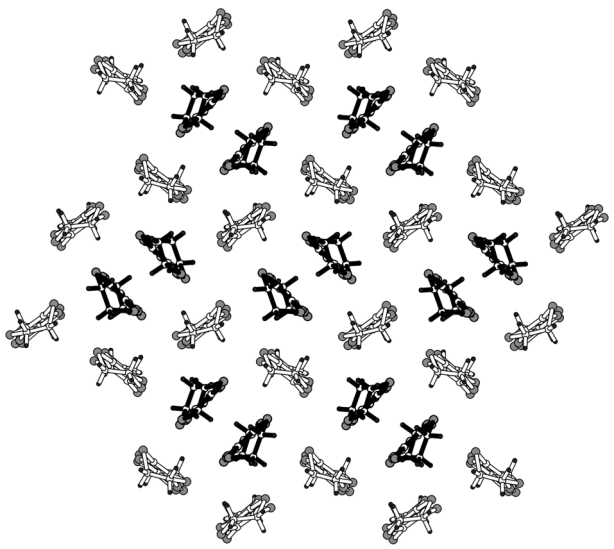

Fig. 3 Conducting BEDT-TTF layer of the 'pseudo-κ' type in the structure of **2**, viewed along the long molecular axis. (BEDT-TTF)$_2^{2+}$ dimers are colored black and surrounded by neutral BEDT-TTF molecules.

Every honeycomb-like anion layer in **2** is racemic, unlike the structure **1**, because it contains both left and right enantiomers of the anion alternating along the *b*-direction. Functional group of the solvent molecule in the structure **1** is directed nearly along the two-fold axis towards the metal atom of the anion (Fig. 2a) while in **2**, the –CN group of PhCN is elongated towards the mixed K^+/H_3O^+ cation and the angle between *b* and –CN is 63.8(2)° (Fig. 2b). The hexagonal cavity in **2** has a more isometric shape and equal Ru–K^+/H_3O^+ distances of 6.272(1) Å, while in the monoclinic phase **1**, the cavity is more extended along the *b*-axis and shows a Ru–K^+/H_3O^+ distance along *b* of 6.379(1) Å which is longer than the two other distances of 6.283(1) Å. The phenyl ring of the solvent lies near the center of the cavity in **2**, while in **1** the phenyl cycle is shifted to one side of the cavity. The dihedral angle between mean planes of the solvent and nearest oxalate bridges is 32.5(5)° in **2** which is much less than that in the monoclinic salt **1**. Ru–O bond distances in the anion are 2.032(2), 2.032(2) and 2.036(2) Å. Relative occupancy of the mixed cation site was refined to 0.69/0.31 for K^+/H_3O^+, respectively. The coordination sphere of the K^+/H_3O^+ cation includes six oxygen atoms of the

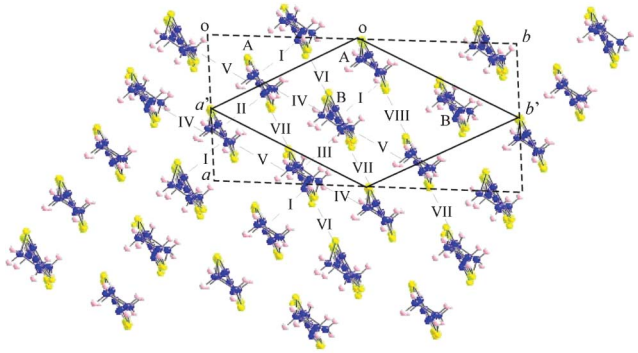

Fig. 4 Schematic representation of the β′′-type donor layer in **1**, where the *a*, *b* and *a*′, *b*′ repeat vectors as well as the different donors (A–B) and intermolecular interactions (I to VIII) are labelled.

oxalate ligands and two nitrogen atoms from PhCN. Distances between K^+/H_3O^+ and oxygen are equal to 2.825(3), 2.883(3) and 2.922(3) Å; K···N distance is 2.979(7) Å.

Electronic structure of β′′-(BEDT-TTF)$_4$K$_x$(H$_3$O)$_{1-x}$[Ru^{III}(ox)$_3$]C$_6$H$_5$Br (1, sample with maximal T_c)

The donor layers of **1** contain two different donors (A and B in Fig. 4) and eight different types of HOMO···HOMO (highest occupied molecular orbital) interactions (see Fig. 4). As far as this layer is considered independently from the anions it can be described as a primitive lattice (instead of *C*-centered in *C*2/*c* space group) using the repeat vectors $a' = (a/2 - b/2)$ and $b' = (a/2 + b/2)$ (see Fig. 4). As for any β′′-type salt, the donor layers of Fig. 4 can be considered to be built from a series of parallel stacks of slipped donors ('slipped-chains'), of step-chains, or of donor chains making lateral π-type HOMO···HOMO interactions ('π-chains'). Interactions I to III are associated with the slipped-chains, IV and V with the step-chains and VI, VII and VIII with the π-chains. The calculated transfer integrals according to the dimer splitting model[27] are reported in Table 1. These values are typical for BEDT-TTF salts of this family:[7] stronger interactions along the step-chains and relatively different values for the interactions along the slipped stacks so that these stacks could be considered as a series of interacting dimers. It is worth noting that the two donors have HOMO energies that are practically identical ($\Delta E \leqslant 10$ meV) so that as far as the HOMO···HOMO interactions are concerned they may be considered identical despite the structural differences (disorder of the ethylene groups in one of them, B). Judging from the values in Table 1 the present salt may be described as a series of A–B BEDT-TTF dimers interacting along all directions of the slab so that this salt should be a two-dimensional (2D) conductor.

The calculated band structure for a donor layer of **1** is shown in Fig. 5. There are four bands mainly based on the HOMO of BEDT-TTF because there are four donors per repeat unit of the layer. The bands in Fig. 5 must contain two holes and since (i) there is no band gap between the two upper bands, and (ii) the dispersion of these bands is quite sizeable, this salt should be metallic in keeping with the experimental results. The calculated Fermi surface contains closed electron pockets around Y and closed hole pockets around X (Fig. 6). The area of these pockets is identical and amounts to 7.5% of the cross section of the Brillouin zone. Note that the partially filled bands are typically 2D in agreement with the analysis above. As analyzed in detail elsewhere,[28] the Fermi surface of β′′-type BEDT-TTF donors results from the hybridization of ellipses with an area of 100% of the cross-section of the Brillouin zone and this is also the case here (see Fig. 7).

Table 1 $t_{HOMO-HOMO}$ transfer integrals (meV) and S···S distances shorter than 3.9 Å for the different donor···donor interactions in a donor layer of **1**

Interaction[a]	S···S (<3.9 Å)	$t_{HOMO-HOMO}$ (meV)
I (A–B)	3.670, 3.801, 3.834, 3.864	−139
II (A–A)	3.751(×2)	−48
III (B–B)	3.834	−57
IV (A–B)	3.617, 3.744, 3.749, 3.809	+203
V (A–B)	3.599, 3.775, 3.785, 3.893	+180
VI (B–B)	3.414(×2), 3.518(×2), 3.836, 3.845(×2)	−97
VII (A–B)	3.321, 3.370, 3.523, 3.555,3.832	−90
VIII (A–A)	3.667(×2), 3.857	−55

[a] See Fig. 4 for the labelling.

Conductivity and magnetotransport measurements

The temperature dependence of the out-of-plane resistivity $\rho_\perp$ for several samples of β′′-(BEDT-TTF)$_4$K$_x$(H$_3$O)$_{1-x}$[Ru^{III}(ox)$_3$]C$_6$H$_5$Br, obtained in the course of the same synthesis, is shown in Fig. 8.

The curve $\rho_\perp(T)$, which corresponds to the highest superconducting critical temperature T_c = 6.3 K (Sample #1), is typical for a layered organic conductor. It has a ''hump'' which separates the regions with the semiconductor-like dependence at higher temperature and the metal-like at lower temperature. The ''hump'' on $\rho_\perp(T)$ dependence is due to the coherent–incoherent transition in the out-of-plane transport in the layered highly anisotropic crystals[29] and its shape is known to

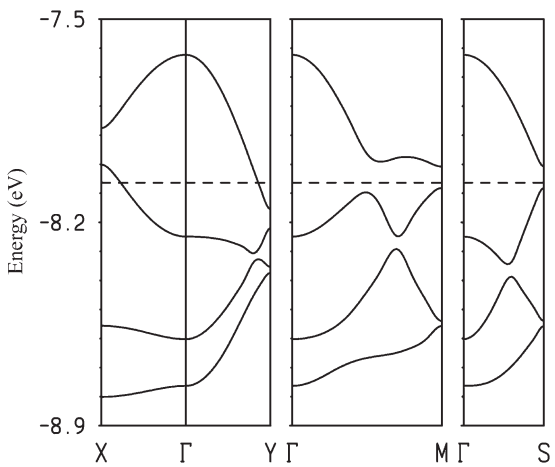

Fig. 5 Band structure calculated for a donor layer of **1**. The dashed line refers to the Fermi level. $\Gamma = (0, 0)$, $X = (a'^*/2, 0)$, $Y = (0, b'^*/2)$. $M = (a'^*/2, b'^*/2)$ and $S = (-a'^*/2, b'^*/2)$ where $a' = (a/2 - b/2)$ and $b' = (a/2 + b/2)$.

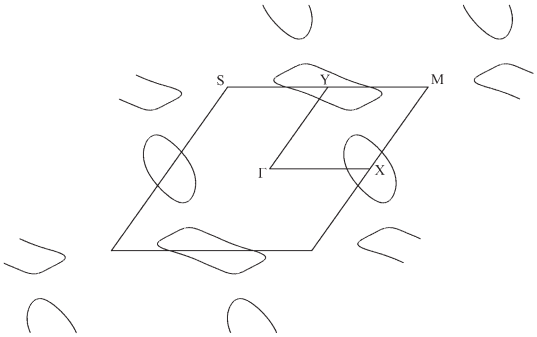

Fig. 6 Fermi surface calculated for a donor layer of **1**.

be sensitive to the impurity scattering.[30,31] As seen from Fig. 8, Sample #1 has the lowest resistivity both at room and at low temperature with respect to the other samples and, besides, has the highest T_c value. For these reasons we consider this sample as the most perfect and uniform. Nevertheless, we believe that the transformation of the $\rho_\perp(T)$ dependency owing to the different sample quality in Fig. 8 is very interesting and impressive, and could be the subject of special study and discussion. Unfortunately our X-ray experiments did not reveal any essential difference between the samples with different $\rho_\perp(T)$ dependencies. We performed full X-ray structural analysis for two samples: #1 with maximal T_c = 6.3 K (this structure is described above) and #4 with minimal T_c = 2.8 K (see ESI†). Both crystals show similar positional disorder and first of all one can suppose different occupancy of disordered positions. However, occupation factors in both samples appeared to be very close: for ethylene groups of the BEDT-TTF they were refined to 0.69/0.31, 0.67/0.33 in #1 and 0.68/0.32, 0.68/0.32 in #4; for K^+/H_3O^+ −0.81/0.19 in #1 and 0.77/0.23 in #4. The electronic band structure calculations have also been carried out for crystal #4 with minimal T_c. The calculated transfer integrals, band structure and Fermi surface are

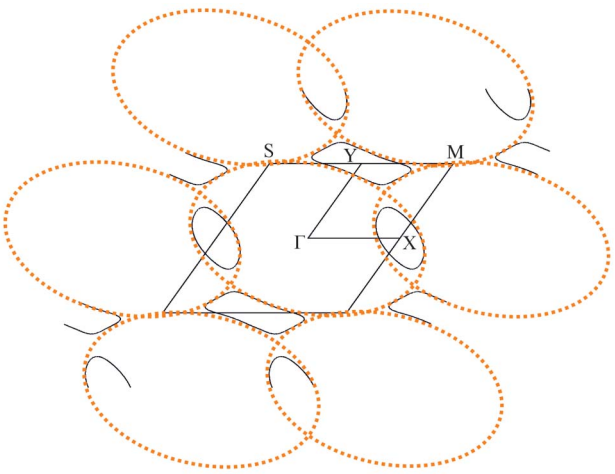

Fig. 7 Schematic representation of the way in which the Fermi surface of Fig. 6 results from the hybridization of a series of superposed ellipses typical of a 2D metal.

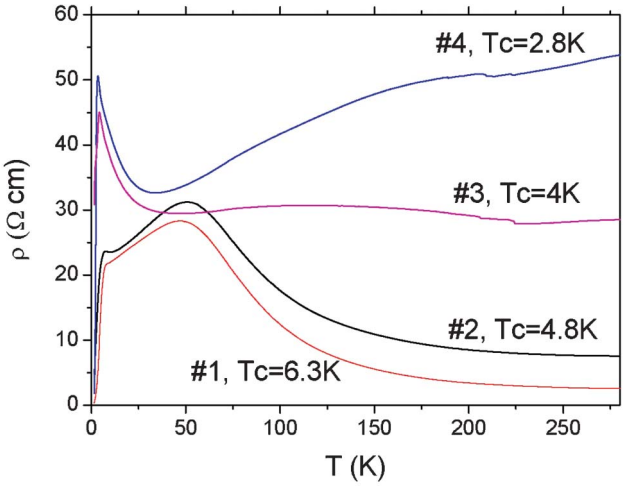

Fig. 8 The temperature dependence of the out-of-plane resistivity $\rho_\perp$ for several samples, obtained in the course of the same synthesis.

reported in the Table S1 and Fig. S3 and S4 of the ESI.† The results are practically indistinguishable from the previous ones obtained for Sample #1 so that we must conclude that there is nothing in the crystal and electronic structure of the donor layers justifying the observed differences in physical behavior, except maybe the actual distribution of the different cationic species on the A^+ sites. We believe that namely the different local arrangements of cations K^+/H_3O^+ could be the reason for the different physical behavior of our samples in spite of their similarity "on average" by X-ray analysis. The different local concentration of cations K^+/H_3O^+ will act in local modifications of the donor layer because donor and anion layers are related through hydrogen bonding and thus affect the electron–phonon coupling constant. As a result, the layer-to-layer disorder may lead to the dielectrization in the interlayer transport just as is seen in Fig. 8 for two upper curves at $T < 40$ K. Moreover, the lowering of the T_c value could be due to the same reason because a random distribution over the layer properties is known to suppress the superconductivity in the out-of plane direction.[32]

The results of the magnetoresistance measurements of Sample #1 at T = 0.4 K are presented in Fig. 9. The magnetic field was oriented perpendicular to the conducting layers. At $B > 7$ T, well pronounced Shubnikov–de Haas oscillations are observed. As seen from the insert to the figure, the Fourier spectrum of oscillations mainly consists of two frequencies: the highest F_1 = 262 T and the lowest F_2 = 35.4 T. There is also a well reproducible small amplitude satellite line with the frequency F_1^* = 224 T. This frequency satisfies with good accuracy to the relationship $F_1^* = F_1 - F_2$. Two main frequencies F_1 and F_2 correspond to the Fermi surface cross sections S1 = 2.5 × 10^{18} m^{-2} and S2 = 3.4 × 10^{17} m^{-2}, *i.e.* 6.3% and 0.85% of the Brillouin zone (BZ) area respectively. The greater cross section value S1 is in satisfactory agreement with the result of electronic structure calculation, according to which the Fermi surface contains two different pockets of the same area of about 7.5% of the BZ (see Section 3). As for the origin of the smaller observed cross section S2, there are two possible explanations: i) the

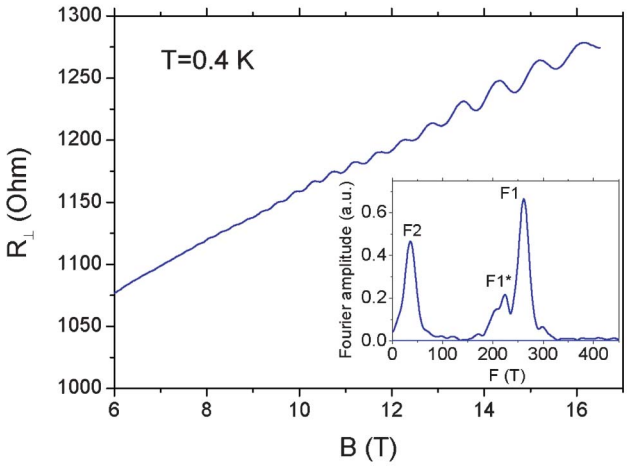

Fig. 9 Shubnikov–de Haas oscillations of the out-of-plane resistance for Sample #1. The Fourier spectrum of oscillations is shown in the insert.

frequency F_2 could be the result of the beating of F_1 and F_1* frequencies which are due to the existence of two extremal cross-sections of the wrapped Fermi-surface, and ii) the frequency F_2 is the consequence of the existence of very small pocket at M (see Fig. 5 and 7) if the corresponding energy levels could be slightly shifted to intersect the Fermi level. For example, this could happen due to the change of the lattice parameters when lowering the temperature. Here we should note that our band structure calculations used the lattice parameters measured at room temperature. The existence of additional small pockets was assumed earlier for Fe oxalate with dimethylformamide solvent where very similar oscillations were detected.[16] In principle, the two explanations are both equally likely, but there is one consideration in favor of the second one. On the basis of density functional theory calculations of the Fermi surface for several molecular organic metals we found that, as a general rule, there is some small warping along the interlayer direction when there are some direct contacts between the donors from adjacent conducting layers or the anion layer is very thin. But when the anion layer is not very thin, the warping is extremely small. For instance, there is some warping in the Bechgaard salts (2–6 meV)[33] or in β-(BEDT-TTF)$_2$IBr$_2$ (around 9 meV).[34] However, in α-(BEDT-TTF)$_2$KHg(SCN)$_4$, where the anion layer is thicker and completely separates the two conducting donor layers, the warping is extremely weak, 0.2 meV.[35] In the salt **1** where the anion layers are thick (the shortest donor···donor contacts are larger than 5.0 Å), we should be in a situation very much like that of the last salt. Thus we believe that the warping of the Fermi surface should be extremely small in **1** and the explanation based on the existence of additional pockets is more likely.

Conclusion

In summary, the crystals of two new compounds belonging to the known family of bifunctional molecular (super)conductors based on BEDT-TTF salts with paramagnetic tris(oxalato)metallate anions (BEDT-TTF)$_4$A^{I}[M^{III}(ox)$_3$]G have been synthesized. Unlike all the known crystals of the family, comprising M^{III} ions of 3d-elements only (Fe, Cr, Mn), the prepared crystals contain the ions of 4d-metal: β′′-(BEDT-TTF)$_4$K$_x$(H$_3$O)$_{1-x}$[Ru^{III}(ox)$_3$]C$_6$H$_5$Br (**1**) and 'pseudo-κ'-(BEDT-TTF)$_4$K$_x$(H$_3$O)$_{1-x}$[Ru^{III}(ox)$_3$]C$_6$H$_5$CN (**2**), where $x \sim 0.8$ (**1**) and 0.7 (**2**). Compound **1** has monoclinic *C*2/*c* symmetry and β′′-packing of the conducting BEDT-TTF layer, whereas the single crystals **2** have orthorhombic *Pbcn* symmetry and 'pseudo-κ' packing of the conducting layers. The crystals were obtained by electrochemical oxidation of BEDT-TTF in the presence of the electrolyte K$_3$[Ru(ox)$_3$]·4.5H$_2$O. Unlike known unsuccessful attempts to synthesize BEDT-TTF salts with [Ru(ox)$_3$]$^{3-}$ anion in the medium of the wet solvent,[6] we used mixtures of solvents: PhBr with 96% EtOH for synthesis of crystals **1** or PhCN with 96% EtOH and 1,2,4-triclorobenzene for **2**.

The study of the temperature dependencies of the out-of-plane resistivity $\rho_\perp$ of **1** shows that these crystals are superconducting, while the crystals **2** exhibit semiconducting behavior. It should be noted that several samples of **1** obtained in the same synthesis have different $\rho_\perp(T)$ behavior and superconducting transition temperatures T_c in the range of 2.8–6.3 K. The full X-ray structural analysis and band structure calculations were made for two samples: with maximal T_c = 6.3 K and with minimal T_c = 2.8 K. Differences in crystal and electronic structures of these samples appeared to be negligible but the observed differences in physical behavior could be explained by the actual distribution of the different cationic species on the A$^+$ sites.

Well pronounced Shubnikov–de Haas oscillations are observed in the field range 7–17 T. The Fourier spectrum of the oscillations mainly consists of two frequencies: the highest F_1 = 262 T and the lowest F_2 = 35.4 T. There is also a well reproducible small amplitude satellite line with the frequency F_1* = 224 T, which equals approximately $F_1 - F_2$. Two main frequencies F_1 and F_2 correspond to the Fermi surface cross sections 6.3% and 0.85% of the Brillouin zone. The first one with good accuracy corresponds to the calculated cross section 7.5%. The F_2 frequency most probably is the consequence of the existence of very small pocket around the *M* point of the Brillouin zone.

Acknowledgements

This work was partially supported by the RFBR grants 12-02-00869, 12-02-00312 and the Program of Russian Academy of Sciences. Work at Bellaterra was supported by the Spanish Ministerio de Economía y Competitividad (Grants FIS2012-37549-C05-05 and CSD2007-00041).

References

1 M. Kurmoo, A. W. Graham, P. Day, S. J. Coles, M. B. Hursthouse, J. L. Caufield, J. Singleton, F. L. Pratt,

W. Hayes, L. Ducasse and P. Guionneau, *J. Am. Chem. Soc.*, 1995, **117**, 12209.
2 L. Martin, S. S. Turner, P. Day, F. E. Mabbs and J. L. McInnes, *Chem. Commun.*, 1997, 1367.
3 S. S. Turner, P. Day, K. M. Abdul Malik, M. B. Hursthouse, S. J. Teat, E. J. MacLean, L. Martin and S. A. French, *Inorg. Chem.*, 1999, **38**, 3543.
4 S. Rashid, S. S. Turner, P. Day, J. A. K. Howard, P. Guionneau, E. J. L. McInnes, F. E. Mabbs, R. J. H. Clark, S. Firth and T. Biggse, *J. Mater. Chem.*, 2001, **11**, 2095.
5 S. Rashid, S. S. Turner, D. Le Pevelen, P. Day, M. E. Light, M. B. Hursthouse, S. Firth and R. J. H. Clark, *Inorg. Chem.*, 2001, **40**, 5304.
6 L. Martin, S. S. Turner, P. Day, P. Guionneau, J. A. K. Howard, D. E. Hibbs, M. E. Light, M. B. Hursthouse, M. Uruichi and K. Yakushi, *Inorg. Chem.*, 2001, **40**, 1363.
7 T. G. Prokhorova, S. S. Khasanov, L. V. Zorina, L. I. Buravov, V. A. Tkacheva, A. A. Baskakov, R. B. Morgunov, M. Gener, E. Canadell, R. P. Shibaeva and E. B. Yagubskii, *Adv. Funct. Mater.*, 2003, **13**, 403.
8 E. Coronado, S. Curelli, C. Giménez-Saiz and C. J. Gómez-García, *Synth. Met.*, 2005, **154**, 245.
9 L. V. Zorina, T. G. Prokhorova, S. V. Simonov, S. S. Khasanov, R. P. Shibaeva, A. I. Manakov, V. N. Zverev, L. I. Buravov and E. B. Yagubskii, *J. Exp. Theor. Phys.*, 2008, **106**, 347.
10 H. Akutsu, A. Akutsu-Sato, S. S. Turner, P. Day, E. Canadell, S. Firth, R. J. N. Clark, J. Yamada and S. Nakatsuji, *Chem. Commun.*, 2004, 18.
11 L. Martin, P. Day, H. Akutsu, J. Yamada, S. Nakatsuji, W. Clegg, R. W. Harrington, P. N. Horton, M. B. Hursthouse, P. McMillan and S. Firth, *CrystEngComm*, 2007, **9**, 865.
12 A. Akutsu-Sato, H. Akutsu, J. Yamada, S. Nakatsuji, S. S. Turner and P. Day, *J. Mater. Chem.*, 2007, **17**, 2497.
13 T. G. Prokhorova, L. I. Buravov, E. B. Yagubskii, L. V. Zorina, S. S. Khasanov, S. V. Simonov, R. P. Shibaeva, A. V. Korobenko and V. N. Zverev, *CrystEngComm*, 2011, **13**, 537.
14 L. V. Zorina, S. S. Khasanov, S. V. Simonov, R. P. Shibaeva, V. N. Zverev, E. Canadell, T. G. Prokhorova and E. B. Yagubskii, *CrystEngComm*, 2011, **13**, 2430.
15 L. V. Zorina, S. S. Khasanov, S. V. Simonov, R. P. Shibaeva, P. O. Bulanchuk, V. N. Zverev, E. Canadell, T. G. Prokhorova and E. B. Yagubskii, *CrystEngComm*, 2012, **14**, 460.
16 A. Audouard, V. N. Laukhin, L. Brossard, T. G. Prokhorova, E. B. Yagubskii and E. Canadell, *Phys. Rev.*, 2004, **B69**, 144523.
17 E. Coronado, S. Curreli, C. Giménez-Saiz and C. J. Gómez-García, *Inorg. Chem.*, 2012, **51**, 1111.
18 R. B. Morgunov, A. A. Baskakov, L. R. Dunin-Barkovskiy, S. S. Khasanov, R. P. Shibaeva, T. G. Prokhorova, E. B. Yagubskiy, T. Kato and Y. Tanimoto, *J. Phys. IV France*, 2004, **114**, 335.
19 J. Larionova, B. Mombelli, J. Sanchiz and O. Kahn, *Inorg. Chem.*, 1998, **37**, 679.
20 Oxford Diffraction, *Xcalibur CCD System, CrysAlisPro Software System, version 1.171.32*, Oxford Diffraction Ltd., 2007.
21 G. M. Sheldrick, *Acta Crystallogr., Sect. A: Found. Crystallogr.*, 2008, **A64**, 112.
22 M.-H. Whangbo and R. Hoffmann, *J. Am. Chem. Soc.*, 1978, **100**, 6093.
23 J. H. Ammeter, H.-B. Bürgi, J. Thibeault and R. Hoffmann, *J. Am. Chem. Soc.*, 1978, **100**, 3686.
24 A. Pénicaud, K. Boubekeur, P. Batail, E. Canadell, P. Auban-Senzier and D. Jérome, *J. Am. Chem. Soc.*, 1993, **115**, 4101.
25 E. Coronado, J. R. Galán-Mascarós, C. Giménez-Saiz, C. J. Gómez-García, J. M. Martínez-Agudo and E. Martínez-Ferrero, *Polyhedron*, 2003, **22**, 2381.
26 E. Coronado, S. Curelli, C. Giménez-Saiz and C. J. Gómez-García, *J. Mater. Chem.*, 2005, **15**, 1429.
27 P. M. Grant, *J. Phys. (Paris)*, 1983, **44**, C3–847.
28 R. Rousseau, M. Gener and E. Canadell, *Adv. Funct. Mater.*, 2004, **14**, 201.
29 J. Merino and R. H. McKenzie, *Phys. Rev. B: Condens. Matter Mater. Phys.*, 2000, **61**, 7996.
30 D. B. Gutman and D. L. Maslov, *Phys. Rev. Lett.*, 2007, **99**, 196602.
31 J. G. Analytis, A. Ardavan, S. J. Blundell, R. L. Owen, E. F. Garman, C. Jeynes and B. J. Powell, *Phys. Rev. Lett.*, 2006, **96**, 177702.
32 M. Dzierzawa, M. Zamora, D. Baeriswyl and X. Bagnoud, *Phys. Rev. Lett.*, 1996, **77**, 3897.
33 (*a*) P. Auban-Senzier, D. Jérome, N. Doiron-Leyraud, S. René de Cotret, A. Sedeki, C. Bourbonnais, L. Taillefer, P. Alemany, E. Canadell and K. Bechgaard, *J. Phys.: Condens. Matter*, 2011, **23**, 345702; (*b*) P. Alemany, J.-P. Pouget and E. Canadell, unpublished results..
34 Y. J. Lee, R. M. Nieminen, P. Ordejón and E. Canadell, *Phys. Rev. B: Condens. Matter Mater. Phys.*, 2003, **67**, 180505.
35 P. Foury-Leylekian, J.-P. Pouget, Y. J. Lee, R. M. Nieminen, P. Ordejón and E. Canadell, *Phys. Rev. B: Condens. Matter Mater. Phys.*, 2010, **82**, 134116.